



Contents lists available at ScienceDirect

Tetrahedron

journal homepage: www.elsevier.com/locate/tet

Dialkoxymethano[60]fullerenes as electron acceptors in thin-film organic solar cells

Mohammed Y. Suleiman^a, Yue Ma^b, Takafumi Nakagawa^c, Hiroshi Ueno^a,
Yutaka Matsuo^{a, b, c, *}

^a School of Chemistry, Northeast Normal University, 5268 Renmin Street, Changchun, Jilin 130024, China

^b Hefei National Laboratory for Physical Sciences at the Microscale, University of Science and Technology of China, 96 Jinzhai Road, Hefei, Anhui 230026, China

^c Department of Mechanical Engineering, School of Engineering, The University of Tokyo, 7-3-1 Hongo, Bunkyo-ku, Tokyo 113-8656, Japan

ARTICLE INFO

Article history:

Received 21 June 2019

Received in revised form

28 July 2019

Accepted 7 August 2019

Available online xxx

Keywords:

Dialkoxymethanofullerenes

Dialkoxyoxadiazolines

Methanofullerene

Organic solar cells

Organic photovoltaics

ABSTRACT

This study presents the synthesis, characterization, and electrochemical properties of four new dialkoxymethanofullerenes, as well as their performance in organic solar cells (OSCs) devices. Dialkoxymethanofullerenes were synthesized in 27%–32% yield by thermolysis of dialkoxyoxadiazolines and reaction with C₆₀ under reflux in toluene. The prepared compounds were then characterized and used for the first time as electron-acceptor materials in thin-film bulk heterojunction OSCs with PBTZT-stat-BDTT-8 as the electron donor material. The devices made with ethoxy-hexyloxymethanofullerene and methoxy-hexyloxymethanofullerene exhibited optimal power conversion efficiencies (PCEs) of 3.79% and 4.65%, with open-circuit voltage of 0.832 and 0.831 V, respectively. In contrast, the devices made with ethoxy-ethoxymethanofullerene and methoxy-ethoxymethanofullerene exhibited very low PCEs of <0.01% for both, indicating a large impact of the substituents on device performance.

© 2019 Elsevier Ltd. All rights reserved.

1. Introduction

Renewed attention has been given to research on organic solar cell (OSC) devices, particularly after recent advances in power conversion efficiency (PCE) over the past couple of years from 11% to in excess of 17% as a result of novel materials and better device engineering [1–4]. For many years, OSCs have attracted great interest [5,6] and have been regarded as a promising technologies for low-cost, sustainable, and renewable photovoltaic devices, thanks to their promising properties [7] and their ability to form light-weight, mechanically flexible, transparent photovoltaic panels by high-speed, low-cost, continuous roll-to-roll manufacturing processes [8,9]. Among all the various photovoltaic technologies, OSCs in particular have the advantage of high-speed manufacturing with a lower thermal budget because no high-temperature processes are needed [4]. OSCs have the smallest environmental impact and the shortest energy payback period, with the shortest time required for

harvesting the energy invested during their life cycle [10,11]. However, the operational stability and PCEs of OSCs require further improvement [12].

PCEs of organic photovoltaic devices are determined by three parameters; open-circuit voltage (V_{OC}), short-circuit current density (J_{SC}), and fill factor (FF). To achieve high PCE, all three of these parameters should be increased [13]. It is possible to increase V_{OC} by either raising the lowest unoccupied molecular orbital (LUMO) level of the acceptor or lowering the highest occupied molecular orbital (HOMO) level of the donor. As for the fullerene acceptor, the LUMO levels can be raised by installing organic addends across the double bonds of C₆₀. The increase in V_{OC} is the result of shrinking the 60 π -electron conjugated system of fullerene to a 58 π -, 56 π -, or 54 π -electron system. J_{SC} can be increased by introducing novel low-bandgap materials that are well matched to the solar spectrum [14]. The FF parameter indicates how “difficult” or “easy” it is for photogenerated carriers to be extracted from a photovoltaic device [15]. To obtain high FF, OSCs with the bulk heterojunction (BHJ) structure are perhaps the best candidate [16]. In such OSCs, the photoactive layer consists of a BHJ blend film of conjugated polymers (electron donors) and organic semiconductors (electron acceptors). The BHJ structure is considered the most promising

* Corresponding author. Department of Mechanical Engineering, School of Engineering, The University of Tokyo, 7-3-1 Hongo, Bunkyo-ku, Tokyo 113-8656, Japan.

E-mail address: matsuo@photon.t.u-tokyo.ac.jp (Y. Matsuo).

<https://doi.org/10.1016/j.tet.2019.130514>

0040-4020/© 2019 Elsevier Ltd. All rights reserved.

strategy because the interpenetrating morphology of the donor and acceptor allows for better exciton generation and dissociation as well as better charge carrier transport in the active layer [16,17]. To improve the performance of OSCs, various strategies have been used, such as controlling and enhancing the morphology of the photoactive layer [18,19]; designing, engineering, and implementing new device architectures [20,21]; employing interfacial layers [1,21]; and synthesizing new derivatives and/or novel donor and acceptor fragments in the photoactive blend [1].

Among the above-mentioned strategies, the synthesis of new organic photovoltaic materials remains the most important because the synthesis of highly tunable optoelectronic properties of organic materials enables precise optimization of the molecular orbital energy levels, absorption spectra, and charge carrier mobilities of these materials [22]. The main aim of synthesizing new materials (particularly new fullerene derivatives) is to develop materials with suitable properties to implement the aforementioned strategies. Fullerene derivative materials have been widely used as semiconductor electron acceptor [23] thanks to their outstanding electron affinity and reversible redox behavior, as well as their excellent electron-transporting properties due to their small reorganization energy for electron transfer [13]. Further improving OSC efficiency through the synthesis of new organic photovoltaic materials is a topic of great significance. Consequently, many fullerenes derivatives have been developed such as PCBM (phenyl C₆₁-butyric acid methyl ester) [24], SIMEFs (bis(silylmethyl)[60]fullerenes) [25], and ICBA (indene-C₆₀ bisadduct). Herein, we report the synthesis, characterization, and electrochemical properties of four new methanofullerene derivatives for use in OSCs (Scheme 1). This is the first report of using dialkoxymethanofullerenes such as C₆₀C(OR)₂ in OSC devices, which gave PCE values up to 4.6% in BHJ OSCs using a PBTZT-stat-BDIT-8 polymer donor system, which is considered one of the most stable OSCs reported to date [26–28].

2. Results and discussion

Four new dialkoxymethanofullerenes C₆₀(CO₂R¹R²) were synthesized in 27%–32% yield by using the method reported by Warrentin and coworkers for oxadiazolines as convenient sources of dialkoxycarbene [29]. The dialkoxymethanofullerenes were exclusively prepared by thermolysis of dialkoxyoxadiazolines (**1**) and reaction with C₆₀ under reflux in toluene (Fig. 1). Starting materials **1** were synthesized in up to 75% yield via oxidative cyclization of alkoxy carbonyl hydrazone of acetone by treatment with iodobenzene diacetate in alcohol ROH (Scheme S1, Supporting Information).

The facile reaction of dialkoxyoxadiazolines with C₆₀ was likely due to the high electrophilicity of C₆₀ and the nucleophilic nature of the dialkoxyoxadiazolines. Methanofullerenes have two possible isomers, namely, a 6-6 closed isomer (σ -homoaromatic) and a 6-5

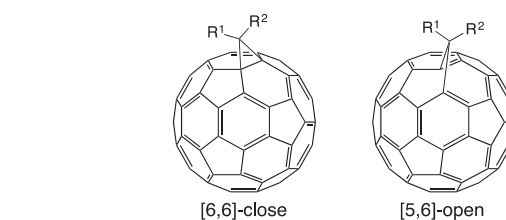
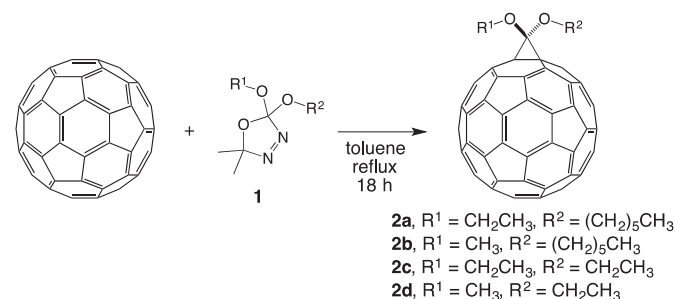


Fig. 1. Two possible isomers of methanofullerenes.

open isomer (π -homoaromatic), with different configurations of the transannular bond (Fig. 1). However, the reaction of C₆₀ with dialkoxyoxadiazolines leads to only the 6-6 open isomer, because the 6-6 ring junction bonds are shorter than the 6-5 ring junction bonds. As a result, the 6-6 closed isomer with a σ -homoaromatic structure is energetically more favorable, and the bridgehead carbon is thus positioned at a smaller distance [30,31]. After considerable experimentation, we found that the presence of excess dialkoxyoxadiazolines reduced the yield of the desired compounds and gave a mixture of mono-, di-, and triadducts, with no trace of the desired products obtained in case of the presence of very large excess dialkoxyoxadiazolines.

A unique property of dialkoxymethanofullerene C₆₀(CO₂R¹R²) is the extensive structural variation that is possible. Variation of the R¹ and R² substituents was utilized to form symmetric and non-symmetric derivatives, namely, ethoxy(hexyloxy)methanofullerene (**2a**), hexyloxy(methoxy)methanofullerene (**2b**), di(ethoxy)methanofullerene (**2c**), and ethoxy(methoxy)methanofullerene (**2d**). These compounds are expected to be useful in a wide variety of studies owing to their diverse chemical and physical properties. Altering the alkyl group substituents allow us to tune the physical properties and the solubility of the molecules in common organic solvents such as toluene. We found that the solubility of **2a** and **2b**, which is an essential requirement for solution-based processes, was relatively high. In contrast, the solubility of **2c** and **2d** was relatively low, which was related to their high crystallinity. The short ethyl chain in the dialkoxy part of **2c** and **2d** may increase their propensity to form partly insoluble aggregates, which negatively affects the thin-film morphology and OSC device performance [32]. These results indicate that a hexyl chain in the dialkoxy part of the dialkoxymethanofullerenes is indispensable for low crystallinity and good solubility.

The electrochemical properties of **2a**, **2b**, **2c**, and **2d** were evaluated by cyclic voltammetry (CV; Fig. 2) and differential pulse voltammetry (DPV; Fig. S9). The LUMO levels of the dialkoxymethanofullerenes, as determined via the electrochemical measurements, are listed in Table 1. The LUMO levels of **2a** and **2b** were



Scheme 1. Synthesis of dialkoxymethanofullerenes.

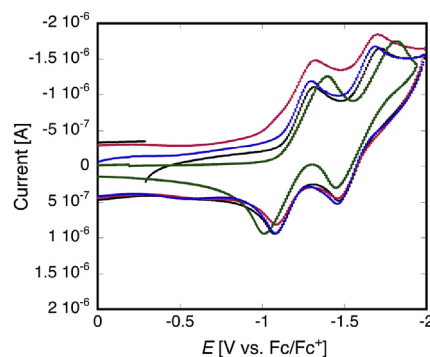


Fig. 2. Cyclic voltammograms of **2a** (black), **2b** (red), **2c** (green), and **2d** (blue) in chlorobenzene containing *n*-Bu₄N⁺PF₆⁻ (0.1 M) as a supporting electrolyte at 25 °C.

Table 1
LUMO levels, solubilities, and electron mobilities of dialkoxymethanofullerenes.

| entry | fullerenes | LUMO levels [eV] ^a | solubility in PhCl [g/mL] ([mol/L]) | electron mobility ^b [cm ² /Vs] |
|-------|---------------------|-------------------------------|-------------------------------------|--|
| 1 | 2a | 3.73 | 79 (9.5 × 10 ⁻²) | 2.5 × 10 ⁻⁵ |
| 2 | 2b | 3.73 | 15 (1.7 × 10 ⁻²) | 3.3 × 10 ⁻⁵ |
| 3 | 2c | 3.58 | 7.0 (8.5 × 10 ⁻³) | — |
| 4 | 2d | 3.53 | 4.2 (5.3 × 10 ⁻³) | — |
| ref | PC ₆₁ BM | 3.8 | — | 3.4 × 10 ⁻⁵ |

^a LUMO levels = $-(4.8 + E_{red1}^{red1})$.

^b The electron-only device structure: ITO/ZnO/active layer (PBTZT-stat-BDIT-8:fullerene)/Al. A reference electron-only device with PC₆₁BM showed 3.4 × 10⁻⁵ cm²/V.

0.15–0.2 eV lower than those of **2c** and **2d**, meaning that **2a** and **2b** were electrochemically superior to **2c** and **2d** as electron acceptors.

Given the promising fundamental properties of the dialkoxymethanofullerenes, we next assessed their OSC performance in standard BHJ devices using a PBTZT-stat-BDIT-8 polymer donor system. The OSC conformation was indium tin oxide (ITO)/poly(3,4-ethylenedioxythiophene):poly(styrenesulfonate) (PEDOT:PSS)/PBTZT-stat-BDIT-8 polymer (Fig. S15):dialkoxymethanofullerene/LiF/Al, and the results are shown in Fig. 3 and Table 2.

The OSC devices using **2a** and **2b** had much higher J_{SC} values of 10.183 and 9.621 mA/cm² with PCEs of 4.65% and 3.79%, respectively, compared with the devices using **2c** and **2d**, which showed negligible J_{SC} of 0.002 and 0.003, respectively, with PCEs of <0.01% for both (Table 2). The relatively high PCEs of the **2a**- and **2b**-based devices were associated with the compounds' relatively high solubility (Table 1), which led to fabrication of thin films with good morphology and then to higher performance for the OSC devices

Table 2
Photovoltaic performance of the devices using fullerene derivatives.

| entry | fullerenes | J_{SC} [mA/cm ²] | V_{OC} [V] | FF [–] | PCE [%] |
|-------|---------------------|--------------------------------|--------------|--------|---------|
| 1 | 2a | 10.183 | 0.832 | 0.447 | 3.79 |
| 2 | 2b | 9.621 | 0.831 | 0.581 | 4.65 |
| 3 | 2c | 0.002 | 0.140 | 0.476 | <0.01 |
| 4 | 2d | 0.003 | 0.440 | 0.345 | <0.01 |
| ref | PC ₆₁ BM | 11.536 | 0.845 | 0.673 | 6.56 |

with these compounds as acceptors. In addition, the good morphology of the thin films facilitated charge generation at the donor–acceptor interface. By contrast, the PCE values of essentially zero for devices using **2c** and **2d** were due to their relatively low solubility, which led to fabrication of thin films with poor morphology. Furthermore, the low solubility of **2c** and **2d** was found to be unsuitable for spin coating. The thin films of **2a** and **2b** had substantially higher film quality in comparison with **2c** and **2d**. This difference can be attributed to the very low crystallinity of **2a** and **2b** due to the presence of the hexyloxy chain and their asymmetric structures. V_{OC} for **2a** and **2b** was substantially and significantly higher than that for **2c** and **2d**, by 0.69–0.39 V. Considering the high V_{OC} (0.83 V) obtained for the devices of **2a** and **2b**, we surmise that the LUMO–LUMO gap between the donor (PBTZT-stat-BDIT-8) and the acceptor is close to the theoretical limit (ca. 0.3 eV) for charge separation [33,34] due to the low-lying LUMO level of PBTZT-stat-BDIT-8. Compounds **2c** and **2d** have shallower LUMO levels than **2a** and **2b**, which may prevent electron transfer from the donor to the acceptor. Electron mobility of electron-only devices with the structure of ITO/ZnO/active layer (PBTZT-stat-BDIT-8:fullerene)/LiF/Al using **2a** and **2b** showed similar electron mobilities as the reference device using PC₆₁BM (Table 1). Overall, all those factors together achieved high PCEs in **2a**- and **2b**-based devices. Although performance of the devices using dialkoxymethano[60]fullerenes were lower than the PCBM device, the authors think the dialkoxymethano[60]fullerenes are tunable and promising materials.

3. Conclusion

In summary, we have designed, synthesized, and characterized new dialkoxymethanofullerenes. These compounds were then utilized as electron acceptors in thin-film OSCs for the first time. The dialkoxymethanofullerenes were prepared with various substitution patterns for the dialkoxy part of the dialkoxymethanofullerenes, namely, ethoxy-hexyloxy, methoxy-hexyloxy, ethoxy-ethoxy, and methoxy-ethoxy substituents, to study the impact of the substituents on thin-film morphology and OSC device performance. The dialkoxymethanofullerenes were used in OSC devices with a structure of ITO/PEDOT:PSS/PBTZT-stat-BDIT-8 polymer:dialkoxymethanofullerenes/LiF/Al. The devices fabricated with ethoxy-hexyloxymethanofullerene and methoxy-hexyloxymethanofullerene exhibited the highest J_{SC} values of

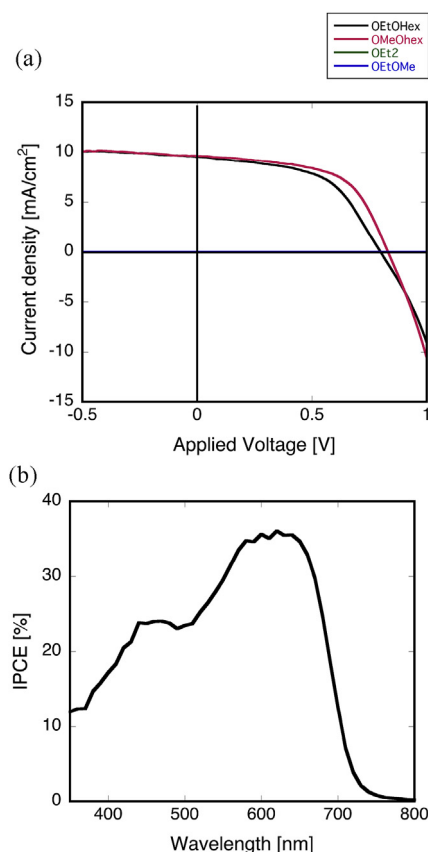


Fig. 3. Photovoltaic performance. (a) Current density–voltage curves of OSC devices based on PBTZT-stat-BDIT-8 polymer: **2a** (black), the polymer: **2b** (red), the polymer: **2c** (green), and the polymer: **2d** (blue). (b) Photocurrent action spectra of OSC devices based on **2a**.

10.183 and 9.621 mA/cm², with V_{OC} of 0.832 and 0.831 V as well as FF of 0.447 and 0.581, giving PCEs of 3.79% and 4.65%, respectively, as a result of good solubility, which enabled the fabrication of thin films with good morphology. By contrast, the devices fabricated with ethoxy-ethoxymethanofullerene and methoxy-ethoxymethanofullerene exhibited very low J_{SC} of 0.002 and 0.003 mA/cm², with V_{OC} of 0.140 and 0.440 V as well as FF of 0.476 and 0.345, respectively, leading to the PCEs of <0.01% for both. For these compounds, poor solubility related to high crystallinity led to poor morphology of the thin films, and then to negligible J_{SC} and ultimately near-zero PCE. For the dialkoxymethanofullerenes examined in this study, a hexyl chain in the dialkoxide part with an asymmetric structure was indispensable for achieving good solubility, leading to good film morphology and then satisfactory PCE.

4. Experimental

4.1. General

C₆₀ was purchased from Frontier Carbon Corporation. Other reagents were used as received without further purification. All solvents were purified using standard procedures. All reactions dealing with air- or wetness-sensitive compounds were carried out in a dry reaction container under nitrogen. Column chromatography was performed on a silica gel column using CS₂ or CH₂Cl₂ as eluent. HPLC analyses were performed on a Shimadzu LC-10A system supplied with UV spectrophotometric detector and equipped using a Buckyprep column (Nacalai Tesque Inc., 4.6 mm ID x 250 mm) with mobile phase of 7:3 v/v mixture of toluene and 2-propanol (flow rate 1 mL/min). ¹H NMR and ¹³C NMR were measured at 600.38 MHz and 150.97 MHz respectively, on a Varian Unity JEOL ECA-500 instrument at 296–299 K. Cyclic voltammetry was performed using a Hokuto Denko HZ-5000 voltammetric analyzer.

4.2. Synthesis of C₆₀C(OCH₂CH₃)(O(CH₂)₅CH₃) (**2a**)

Under a nitrogen atmosphere, a solution of C₆₀ (200 mg, 0.278 mmol) and oxadiazolines (204 mg, 0.834 mmol) in toluene (100 mL) was refluxed for 18 h under stirring. After removal of solvent by rotary evaporation, the reaction mixture was diluted with CS₂ and subjected to silica gel column chromatography (eluent, CS₂) to remove remaining C₆₀ and separates all of mono-, di-, and triadducts from each other to obtain the crude product. Purification by Buckyprep column separation (eluent: toluene/2-propanol = 7/3) was executed to obtain **2a** which was washed with MeOH, dissolved in toluene, reprecipitated with MeOH, and dried to obtain the target dark red crystal (76 mg, 0.086 mmol, 31% isolated yield, analytically pure). ¹H NMR (600 MHz, CDCl₃): δ 0.94 (t, 3H, OCH₂CH₂CH₂CH₂CH₂CH₃), 1.39 (t, 3H, OCH₂CH₃), 1.51–1.54 (m, 4H, OCH₂CH₂CH₂CH₂CH₂CH₃), 1.55–1.57 (m, 2H, OCH₂CH₂CH₂CH₂CH₂CH₃), 1.86–1.88 (m, 2H, OCH₂CH₂CH₂CH₂CH₂CH₃), 4.26 (t, 2H, OCH₂CH₂CH₂CH₂CH₂CH₃CH₂), 4.32 (q, 2H, OCH₂CH₃). ¹³C{¹H} NMR (150 MHz, CS₂-CDCl₃): δ 145.40, 145.13, 145.01, 144.87, 144.80, 144.68, 144.63, 144.29, 144.26, 143.66, 143.37, 143.14, 142.95, 142.55, 142.52, 142.34, 141.36, 137.68, 137.67. The remaining resonances at 84.54, 68.09, 63.97, 32.07, 30.12, 26.36, 23.23, 15.61, and 14.53 belong to the fullerene-sp³ C-atoms, and dialkoxy C-atoms. We appointed the peak at 96.33 to the bridgehead C-atom. MALDI-TOF-HRMS (+) (m/z): Calcd for C₆₉O₂H₁₈ (M + H⁺): 879.1387, found 879.1382.

4.3. Synthesis of C₆₀C(OCH₃)(O(CH₂)₅CH₃) (**2b**)

Under a nitrogen atmosphere, a solution of C₆₀ (200 mg,

0.278 mmol) and oxadiazolines (192 mg, 0.834 mmol) in toluene (100 mL) was refluxed for 18 h under stirring. After removal of solvent by rotary evaporation, the reaction mixture was diluted with CS₂ and subjected to silica gel column chromatography (eluent, CS₂) to remove remaining C₆₀ and separates all of mono-, di-, and triadducts from each other to obtain the crude product. Purification by Buckyprep column separation (eluent: toluene/2-propanol = 7/3) was executed to obtain **2b** which was washed with MeOH, dissolved in toluene, reprecipitated with MeOH, and dried to obtain the target dark red crystal (77 mg, 0.089 mmol, 32% isolated yield, analytically pure). ¹H NMR (600 MHz, CDCl₃): δ 0.94 (t, 3H, OCH₂CH₂CH₂CH₂CH₂CH₃), 1.38–1.43 (m, 4H, OCH₂CH₂CH₂CH₂CH₂CH₃), 1.52–1.59 (m, 2H, OCH₂CH₂CH₂CH₂CH₂CH₃), 1.86–1.90 (m, 4H, OCH₂CH₂CH₂CH₂CH₂CH₃), 3.97 (s, 3H, OCH₃), 4.25 (t, 2H, OCH₂CH₂CH₂CH₂CH₂CH₃CH₂). ¹³C{¹H} NMR (150 MHz, CS₂-CDCl₃): δ 145.35, 145.12, 145.01, 144.88, 144.85, 144.81, 144.48, 144.32, 144.26, 143.63, 143.41, 143.40, 143.16, 142.94, 142.52, 142.50, 142.36, 141.39, 141.38, 137.78, 137.70. The remaining resonances at 84.65, 68.11, 54.81, 32.10, 30.16, 26.40, 23.27, and 14.58 belong to the fullerene-sp³ C-atoms and dialkoxy C-atoms. We appointed the peak at 96.76 to the bridgehead C-atom. MALDI-TOF-HRMS (+) (m/z): Calcd for C₆₈O₂H₁₆ (M + H⁺): 865.1230, found 865.1225.

4.4. Synthesis of C₆₀C(OCH₂CH₃)₂ (**2c**)

Under a nitrogen atmosphere, a solution of C₆₀ (200 mg, 0.278 mmol) and oxadiazolines (157 mg, 0.834 mmol) in toluene (100 mL) was refluxed for 18 h under stirring. After removal of solvent by rotary evaporation, the reaction mixture was diluted with CS₂ and subjected to silica gel column chromatography (eluent, CS₂) to remove remaining C₆₀ and separates all of mono-, di-, and triadducts from each other to obtain the crude product. Purification by Buckyprep column separation (eluent: toluene/2-propanol = 7/3) was executed to obtain **2c** which was washed with MeOH, dissolved in toluene, reprecipitated with MeOH, and dried to obtain the target dark red crystal (65 mg, 0.079 mmol, 28% isolated yield, analytically pure). ¹H NMR (600 MHz, CDCl₃): δ 1.54 (t, 6H, OCH₂CH₃), 4.37 (q, 4H, OCH₂CH₃). ¹³C{¹H} NMR (150 MHz, CS₂-CDCl₃): δ 145.39, 145.14, 145.02, 144.87, 144.81, 144.64, 144.29, 144.28, 143.66, 143.38, 143.15, 142.95, 152.55, 142.35, 141.37, 137.70. The remaining resonances at 84.57, 64.02, and 15.64 belong to the fullerene-sp³ C-atoms and dialkoxy C-atoms. We appointed the peak at 96.46 to the bridgehead C-atom. MALDI-TOF-HRMS (+) (m/z): calcd for C₆₅O₂H₁₀ (M + H⁺): 823.0761, found 823.0758.

4.5. Synthesis of C₆₀C(OCH₃)(OCH₂CH₃) (**2d**)

Under a nitrogen atmosphere, a solution of C₆₀ (200 mg, 0.278 mmol) and oxadiazolines (145 mg, 0.834 mmol) in toluene (100 mL) was refluxed for 18 h under stirring. After removal of solvent by rotary evaporation, the reaction mixture was diluted with CS₂ and subjected to silica gel column chromatography (eluent, CS₂) to remove remaining C₆₀ and separates all of mono-, di-, and triadducts from each other to obtain the crude product. Purification by Buckyprep column separation (eluent: toluene/2-propanol = 7/3) was executed to obtain **2d** which was washed with MeOH, dissolved in toluene, reprecipitated with MeOH, and dried to obtain the target dark red crystal (60 mg, 0.074 mmol, 27% isolated yield, analytically pure). ¹H NMR (600 MHz, CDCl₃): δ 1.54 (t, 3H, OCH₂CH₃), 4.01 (s, 3H, CH₃), 4.36 (q, 2H, OCH₂CH₃). ¹³C{¹H} NMR (150 MHz, CS₂-CDCl₃): δ 145.34, 145.33, 145.13, 145.02, 144.88, 144.85, 144.81, 144.48, 144.72, 143.63, 143.42, 143.40, 143.17, 142.95, 142.54, 142.52, 142.37, 141.40, 141.38, 137.80, 137.71. The remaining

resonances at 84.67, 64.08, 54.83 and 15.64 belong to the fullerene- sp^3 C-atoms and dialkoxy C-atoms. We appointed the peak at 96.46 to the bridgehead C-atom. MALDI-TOF-HRMS (+) (m/z): calcd for $C_{64}O_2H_8$ (M^+): 808.0524, found 808.0520.

4.6. Device fabrication and evaluation

Fabrication and evaluation of BHJ OSCs: Regioregular Merck polymer and PEDOT:PSS (H.C. Starck, Clevis PVP AI4083) were purchased from Aldrich and H.C. Starck, respectively, and used as received. Active-layer solutions were prepared by using Merck polymer and dialkoxymethanofullerenes in a 1:1 wt ratio (concentration, 20 mg/mL in PhCl). These blended solutions were heated at 80 °C for 1 h under nitrogen, and filtered with poly(tetrafluoroethylene) (pore size, 0.45 μ m) prior to use. All the devices were fabricated on patterned ITO substrates that were ultrasonically cleaned using a surfactant, rinsed with deionized water, dried at 120 °C for 5 min, and subjected to UV-ozone treatment. A thin layer of PEDOT:PSS was spin-coated onto the ITO glass by using an aqueous dispersion of PEDOT:PSS to obtain a smooth 40 nm thick film. The PEDOT:PSS-coated substrate was dried in air for 10 min at 120 °C, and then dried in a nitrogen glove-box for 3 min at 180 °C prior to use. A blended solution of Merck polymer:dialkoxymethanofullerenes was spin-coated onto the PEDOT:PSS layer to obtain an active layer 200 nm thick. Thermal annealing was performed at 100 °C for 10 min under nitrogen. The LiF/Al electrode (LiF = 10 nm; Al = 80 nm) was evaporated onto the film through a shadow mask, giving a device with an active area of 0.25 cm². The solar cell was then encapsulated with backing glass using UV-curable resin under nitrogen. The encapsulated solar cells were subjected to J - V measurements under both dark and irradiated conditions. Current-voltage sweeps were taken with a Keithley 2400 source measurement unit controlled by a computer. The light source used to determine PCE was an AM1.5G solar simulator system (Sumitomo Heavy Industries Advanced Machinery) with an intensity of 100 mW cm⁻².

4.7. SCLC measurements

The mobility was determined by fitting the dark current to a model of a single-carrier SCLC, which is described by the equation: $J = (9/8)\epsilon_0\epsilon_r\mu(V^2/L^3)$, where J is the current density, μ is the mobility, ϵ_0 is the permittivity of free space, ϵ_r is the relative permittivity of the material, L is the thickness of the FA compound layer, and V is the effective voltage. The thickness of the thin films was measured with a DEKTAK 6 M stylus profilometer. A mixture of PBTZT-stat-BDIT-8 polymer: **2a** and **2b** were spin-coated onto the ZnO layer to form a thin film in electron-only devices. The LiF/Al electrodes (LiF = 0.6 nm; Al = 100 nm) were evaporated onto the active layer. The experimental dark current density J was measured under an applied voltage swept from -1 to 5 V.

Acknowledgments

This work was supported by the thousand talent program in Northeast Normal University. This work was also supported by the

Grants-in-Aid for Scientific Research (JSPS KAKENHI Grant Numbers JP15H05760, JP16H04187), MEXT, Japan.

Appendix A. Supplementary data

Supplementary data to this article can be found online at <https://doi.org/10.1016/j.tet.2019.130514>.

References

- [1] S. Rafique, S.M. Abdullah, K. Sulaiman, M. Iwamoto, *Renew. Sustain. Energy Rev.* 84 (2018) 43.
- [2] N. Agrawal, M.Z. Ansari, A. Majumdar, R. Gahlot, N. Khare, *Sol. Energy Mater. Sol. Cells* 157 (2016) 960.
- [3] G. Zhang, K. Zhang, Q. Yin, X.-F. Jiang, Z. Wang, J. Xin, W. Ma, H. Yan, F. Huang, Y. Cao, *J. Am. Chem. Soc.* 139 (2017) 2387.
- [4] S. Sachdeva, J. Kaur, K. Sharma, S. Tripathi, *Curr. Appl. Phys.* 18 (2018) 1592.
- [5] Y. Lin, S. Dong, Z. Li, W. Zheng, J. Yang, A. Liu, W. Cai, F. Liu, Y. Jiang, T.P. Russell, *Nano Energy* 46 (2018) 428.
- [6] R. Bhargava, S. Gairola, A. Patra, S. Naqvi, S. Dhawan, *Opt. Mater.* 80 (2018) 138.
- [7] C. Cui, Y. Li, Y. Li, *Adv. Energy Mater.* 7 (2017) 1601251.
- [8] J. Tong, S. Xiong, Y. Zhou, L. Mao, X. Min, Z. Li, F. Jiang, W. Meng, F. Qin, T. Liu, *Mater. Horiz.* 3 (2016) 452.
- [9] Z. Khezripour, F.F. Mahani, A. Mokhtari, *Opt. Mater.* 84 (2018) 651.
- [10] C. Roldán-Carmona, O. Malinkiewicz, A. Soriano, G.M. Espallargas, A. Garcia, P. Reinecke, T. Kroyer, M.I. Dar, M.K. Nazeeruddin, H.J. Bolink, *Energy Environ. Sci.* 7 (2014) 994.
- [11] B. Azzopardi, C.J. Emmott, A. Urbina, F.C. Krebs, J. Mutale, J. Nelson, *Energy Environ. Sci.* 4 (2011) 3741.
- [12] T. Guo, M. Li, Z. Qiao, L. Yu, J. Zhao, N. Feng, P. Shi, X. Wang, X. Pu, H. Wang, *Superlattice Microstruct.* 117 (2018) 215.
- [13] T. Umeyama, S. Takahara, S. Shibata, K. Igarashi, T. Higashino, K. Mishima, K. Yamashita, H. Imahori, *RSC Adv.* 8 (2018) 18316.
- [14] Y. Matsuo, J. Kawai, H. Inada, T. Nakagawa, H. Ota, S. Otsubo, E. Nakamura, *Adv. Mater.* 25 (2013) 6266.
- [15] B. Qi, J. Wang, *Phys. Chem. Chem. Phys.* 15 (2013) 8972.
- [16] Q. An, F. Zhang, J. Zhang, W. Tang, Z. Deng, B. Hu, *Energy Environ. Sci.* 9 (2016) 281.
- [17] S.A. Ayoub, J.B. Lagowski, *Mater. Des.* 156 (2018) 558.
- [18] W. Ma, J.R. Tumbleston, L. Ye, C. Wang, J. Hou, H. Ade, *Adv. Mater.* 26 (2014) 4234.
- [19] P. Cheng, J. Hou, Y. Li, X. Zhan, *Adv. Energy Mater.* 4 (2014) 1301349.
- [20] Z. He, B. Xiao, F. Liu, H. Wu, Y. Yang, S. Xiao, C. Wang, T.P. Russell, Y. Cao, *Nat. Photonics* 9 (2015) 174.
- [21] Z. Yin, J. Wei, Q. Zheng, *Adv. Sci.* 3 (2016) 1500362.
- [22] W. Zhao, S. Li, H. Yao, S. Zhang, Y. Zhang, B. Yang, J. Hou, *J. Am. Chem. Soc.* 139 (2017) 7148.
- [23] R. Ganesamoorthy, G. Sathiyam, P. Sakthivel, *Sol. Energy Mater. Sol. Cells* 161 (2017) 102.
- [24] J.C. Hummelen, B.W. Knight, F. LePeq, F. Wudl, J. Yao, C.L. Wilkins, *J. Org. Chem.* 60 (1995) 532.
- [25] Y. Matsuo, A. Iwashita, Y. Abe, C.-Z. Li, K. Matsuo, M. Hashiguchi, E. Nakamura, *J. Am. Chem. Soc.* 130 (2008) 15429.
- [26] S. Berny, N. Blouin, A. Distler, H.J. Egelhaaf, M. Krompiec, A. Lohr, O.R. Lozman, G.E. Morse, L. Nanson, A. Pron, *Adv. Sci.* 3 (2016) 1500342.
- [27] I. Jeon, C. Delacou, H. Okada, G.E. Morse, T.-H. Han, Y. Sato, A. Anisimov, K. Suenaga, E.I. Kauppinen, S. Maruyama, *J. Mater. Chem.* 6 (2018) 14553.
- [28] I. Jeon, R. Sakai, S. Seo, G.E. Morse, H. Ueno, T. Nakagawa, Y. Qian, S. Maruyama, Y. Matsuo, *J. Mater. Chem.* 6 (2018) 5746.
- [29] M. El-Saidi, K. Kassam, D.L. Pole, T. Tadey, J. Warkentin, *J. Am. Chem. Soc.* 114 (1992) 8751.
- [30] W. Win, M. Kao, M. Eiermann, J. McNamara, F. Wudl, D. Pole, K. Kassam, J. Warkentin, *J. Org. Chem.* 59 (1994) 5871.
- [31] L. Isaacs, F. Diederich, *Helv. Chim. Acta* 76 (1993) 2454.
- [32] T. Umeyama, K. Igarashi, D. Sakamaki, S. Seki, H. Imahori, *Chem. Commun.* 54 (2018) 405.
- [33] G. Dennler, M.C. Scharber, C.J. Brabec, *Adv. Mater.* 21 (2009) 1323.
- [34] D. Baran, T. Kirchartz, S. Wheeler, S. Dimitrov, M. Abdelsamie, J. Gorman, R. Ashraf, S. Holliday, A. Wadsworth, N. Gasparini, *Energy Environ. Sci.* 9 (2016) 3783.